Nonlocal Electron Heat Transport in Magnetized Dense Plasmas

Akio NISHIGUCHI

Osaka Institute of Technology, Osaka 535-8585, Japan

(Received 20 November 2013 / Accepted 8 May 2014)

Nonlocal electron heat transport in magnetized dense plasmas is studied numerically using a nonlinear Fokker–Planck (FP) model with self-consistent electric fields. The nonlocal effect in electron heat transport is evaluated by comparison with the effective mean free path and the scale length of the temperature gradient. The dependence of the nonlocal electron heat transport on the effective mean free path is shown in this study. Under a very strong magnetic field, the effective electron mean free path becomes shorter than the scale length of the temperature gradient and the results of the FP and linear models agree well. Under a very strong magnetic field, the electron distribution is described by the Maxwell–Boltzmann distribution.

Keywords: nonlocal electron heat transport, magnetic field, high-temperature dense plasma, Fokker–Planck, laser fusion

DOI: 10.1585/pfr.9.1404096

1. Introduction

Electron heat transport plays an important role in laser-produced plasmas. For example, high-density compression is critical to the ignition in laser fusion, where efficient electron heat transport and uniform implosion are crucial. High-density compression is sensitive to preheating and uniformity, which strongly depend on heat transport. In laser produced plasmas, a magnetic field will be important because it implicates transport and nonuniformities. Spontaneously generated magnetic fields in laser-produced plasmas have been experimentally observed and theoretically demonstrated [1–11]. However, to directly detect the magnetic field B is difficult in collisional overdense plasma. Many theoretical studies of electron heat transport in the region have not been taking it into consideration. The high electron heat flux in overdense plasma supplies free energy to the instability that generates the magnetic fields. The well-known $\nabla T \times \nabla n$ effect arising from nonuniform laser illuminations and fluid instabilities, such as Rayleigh–Taylor (RT) and/or Kelvin–Helmholtz, can generate megagauss magnetic fields. The RT instability is a major magnetic field source in imploded plasmas in acceleration and deceleration phases. In particular, in the deceleration phase, magnetic fields are rapidly compressed and amplified; thus, they become sufficiently strong and affect the electron heat transport. The smoothing of nonuniformities depends on how the electron heat transport interacts with magnetic fields. Therefore, the coupled study of electron transport and magnetic field in the region is important. Theoretical studies are complicated by a steep temperature gradient, where the nonlocal description of electron transport is required. The nonlocal electron heat transport in magnetized laser plasmas has been previously investigated [12–15], where the nonlocal electron heat transport between the laser hot spot and the ablation front was studied. For a very strong magnetic field, it is suggested that the nonlocal effect perpendicular to the magnetic field almost vanishes.

A strong self-generated magnetic field is present in laser fusion plasma. In the Fast Ignition of inertial confinement fusion, an external magnetic field is applied to control and guide the high-energy electron transport toward the compressed core plasma. To perform calculations with the required accuracy, analyzing the nonlocal electron heat transport in a magnetic field in three dimensions is necessary. However, the calculation of the three-dimensional nonlinear Fokker–Planck (FP) model using self-consistent E and B fields is very difficult. Therefore, in this study, the nonlinear kinetics of the electron transport in magnetized dense plasmas and the dependence of the electron heat transport on the magnetic field strength are analyzed and clarified. The results are expected to help simplify the models of the nonlocal electron heat transport across a magnetic field.

In this study, the calculations of the nonlinear kinetics of the electron transport in magnetized dense plasmas are described. Although the magnetic field will arise due to multidimensional effects, the calculation is restricted to one dimension for simplicity. Thus, the self-generation of the magnetic field is not considered. Instead, an externally imposed source of the magnetic field is assumed. The magnetic field is spatially uniform and constant over time. The interaction of the magnetic field and the nonlinear heat flux in a steep temperature gradient is studied numerically.

In the past, nonlocal transport in a steep temperature gradient has been found to substantially alter the heat flux relative to the predictions of linear transport theory [16–20]. In this study, it is investigated how the magnetic field affects the nonlocal electron heat transport. The non-

author's e-mail: nisiguti@elc.oit.ac.jp

local effects on electron transport are examined under a magnetic field of variable strength as compared with models that use Braginskii's transport coefficients. In the following sections, the numerical model is described and the results are presented.

2. Numerical Modeling

A slab of uniform dense plasma with a steep temperature gradient is considered. Fixed ions and only one-dimensional spatial inhomogeneity are assumed. At a high temperature, where the influence of the nonlocal heat transport is notable, the time scale of heat transport is much shorter than that of ion motion. Therefore, the effect of ion motion is expected to be negligible.

The transport of electrons is described with the kinetics equation as follows:

$$\frac{\partial f}{\partial t} + \boldsymbol{v} \cdot \nabla f - \frac{e}{m_\mathrm{e}}(\boldsymbol{E} + \boldsymbol{v} \times \boldsymbol{B}) \cdot \nabla_v f = C_\mathrm{collision}, \quad (1)$$

where f is the distribution function, $\boldsymbol{v}$ is the particle velocity, $\boldsymbol{E}$ is the electric field, and $\boldsymbol{B}$ is the magnetic field. A first-order Cartesian tensor expansion for the distribution function is adopted,

$$\begin{aligned} f(\boldsymbol{r}, \boldsymbol{v}, t) &= f_0(\boldsymbol{r}, v, t) + (\boldsymbol{v}/v) \cdot \boldsymbol{f}_1(\boldsymbol{r}, v, t) \\ &= f_0 + (v_x/v) f_x + (v_z/v) f_z. \end{aligned}$$

The dense plasma is expected to be sufficiently collisional, which renders the high-order terms insignificant. The most dominant effect on electron transport is the distortion of the isotropic part of the distribution function f_0 from the Maxwellian [16–18].

The flux-carrying part of the distribution function $\boldsymbol{f}_1$ has two components: f_z, which is parallel to ∇T_e, and f_x, which is perpendicular to both ∇T_e and $\boldsymbol{B}$. The substitution of the above expansion with FP collision into Eq. (1) gives a coupled set of equations for f_0, f_x, and f_z, which can be written as follows:

$$\begin{aligned} &\frac{\partial f_0}{\partial t} + \frac{v}{3}\frac{\partial f_z}{\partial z} - \frac{eE_x}{3m_\mathrm{e}}\frac{1}{v^2}\frac{\partial}{\partial v}(v^2 f_x) - \frac{eE_z}{3m_\mathrm{e}}\frac{1}{v^2}\frac{\partial}{\partial v}(v^2 f_z) \\ &\quad = \frac{1}{v^2}\frac{\partial}{\partial v}\left\{Y\left[Cf_0 + D\frac{\partial f_0}{\partial v}\right]\right\}, \quad (2a) \end{aligned}$$

$$f_x = -\frac{\tau}{1+\chi^2}\left[v\chi\frac{\partial f_0}{\partial z} - \left(\frac{eE_x}{m_\mathrm{e}} + \chi\frac{eE_z}{m_\mathrm{e}}\right)\frac{\partial f_0}{\partial v}\right], \quad \text{and} \quad (2b)$$

$$f_z = -\frac{\tau}{1+\chi^2}\left[v\frac{\partial f_0}{\partial z} + \left(\chi\frac{eE_x}{m_\mathrm{e}} - \frac{eE_z}{m_\mathrm{e}}\right)\frac{\partial f_0}{\partial v}\right], \quad (2c)$$

where

$$\omega = \frac{eB}{m_\mathrm{e}}, \quad \chi(v) = \omega\tau(v),$$

$$\tau = \frac{v^3}{D_\perp v^3 + Zn_\mathrm{e}Y}, \quad Y = \frac{4\pi e^2 \ln\Lambda}{(4\pi\varepsilon_0 m_\mathrm{e})^2},$$

$$C = I_0^0, \quad D = \frac{v}{3}(I_2^0 + J_{-1}^0),$$

$$D_\perp = \frac{n_\mathrm{e}Y}{v^3}\left(I_0^0 - \frac{I_2^0}{3} - \frac{2}{3}J_{-1}^0\right),$$

$$I_j^i = \frac{4\pi}{v^j}\int_0^v f_i u^{j+2} du, \quad J_j^i = \frac{4\pi}{v^j}\int_v^\infty f_i u^{j+2} du.$$

In deriving these equations, the time derivative of $\boldsymbol{f}_1$ is ignored.

From the current moments of Eqs. (2b) and (2c), and assuming $j_z = 0$, Ohm's law for E_x is obtained as follows:

$$E_x = \frac{m_\mathrm{e}}{e}(v_N\omega - \eta j_x). \quad (3)$$

The current j_x is given as follows:

$$j_x = \frac{1}{3}\int_0^\infty v^3 f_x dv,$$

and η and v_N for arbitrary f_0 are given as follows:

$$\eta = \frac{-3}{V_v^3 \Omega}, \quad v_N = \frac{U_z^4 V_v^3 - V_z^4 U_v^3}{V_v^3 V_v^3 \Omega},$$

where

$$\Omega = 1 + \left(\frac{\omega U_v^3}{V_v^3}\right)^2, \quad V_\alpha^i = \int_0^\infty \frac{v^i \tau}{1+\chi^2}\frac{\partial f_0}{\partial \alpha} dv,$$

$$U_\alpha^i = \int_0^\infty \frac{v^i \tau^2}{1+\chi^2}\frac{\partial f_0}{\partial \alpha} dv.$$

The calculation proceeds according to Ref. [14]. Here, f_0 and E_z are defined at n integer time steps, while ω and E_x at half-integer time steps $n + \frac{1}{2}$. By substituting f_x and f_z in Eq. (2a) using Eqs. (2b) and (2c), f_0 is advanced in time. The new E_z is obtained from the current moment of Eq. (2c) and the condition $j_z = 0$. The calculation is repeated until j_z at the new time step is smaller than some set tolerance. The electric field E_x is calculated from Eq. (3). This cycle is repeated in the next time step.

The f_0 equation is differenced to ensure the conservation of number density. Identifying j with velocity indices, the values of C and D are evaluated according to Ref. [21] as follows:

(i) $C_{j+\frac{1}{2}} = \sum_{i=1}^{j}(v^2 f_0)_i dv, \quad 1 < j < JM,$

(ii) $(vD)_{j+\frac{1}{2}} - (vD)_{j-\frac{1}{2}} = (v^2 dv)_j \sum_{i=j}^{JM-1}(vf_0)_{i+\frac{1}{2}} dv$, and

(iii) $(vD)_{\frac{1}{2}} = (v^2 dv)_1 \sum_{i=1}^{JM-1}(vf_0)_{i+\frac{1}{2}} dv.$

This anticipates the cancelation in considering the energy moment of the collision operator.

For the results presented below, 100 velocity groups and 50 spatial mesh points are used. The Braginskii's descriptions [22] are used in the linear transport model.

3. Nonlocal Electron Heat Transport under a Magnetic Field

First, the result of the electron heat transport at low temperature is presented. The initial temperatures of the

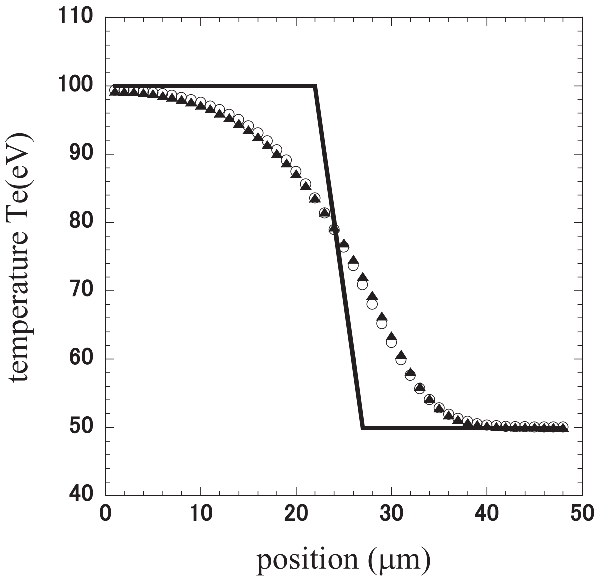

Fig. 1 The temperature profiles at the initial time (solid line) and 10 ns by using the FP (circles) and linear models (filled triangles).

two layers are 100 eV and 50 eV, respectively. The initial temperature profile is indicated by a solid line in Fig. 1. The temperatures vary linearly in a 5 μm thick layer. For simplicity, a fully ionized DT plasma is assumed. The density is spatially uniform and constant over time. The electron density is 10^{24} cm^{-3}. The applied magnetic field is zero. A continuous boundary condition is imposed on both boundaries.

The results of the temperature profiles of the FP and linear models at 10 ns are denoted by circles and filled triangles, respectively, in Fig. 1. In the calculations, the initial temperatures are low; thus, the electron mean free pass is much shorter than the scale length of the temperature gradient L_t. The results of the FP and linear models agree well. The electron distribution function is almost Maxwellian anywhere.

The electron heat transport in a steep temperature gradient is investigated for magnetized dense plasmas produced by implosion in laser fusion. The investigation parameters vary widely, and the results are explained using examples. The initial temperatures of the two layers are 20 keV and 10 keV, respectively. The temperatures vary linearly in a 5 μm thick layer from 20 keV to 10 keV, as indicated by a solid line in Fig. 2. The electron density is 10^{24} cm^{-3}. The electron mean free path at 20 keV is about 8 μm. The scale length of the initial temperature gradient is about 5 μm. The electron heat transport is mainly governed by the electrons, which have energy several times larger than the average temperature, and the mean free path of the electrons is longer than the scale length of the initial temperature gradient. To investigate the influence of the magnetic field on the nonlocal electron heat transport, the magnitude of the magnetic field is varied from zero to 10 MG in the calculations. The imposed magnetic field is spatially uniform and constant over time.

The temperature profiles of the FP and linear models for four different B are shown in Fig. 2. Figure 2 (a) shows the temperature profiles at 0.05 ps for the zero magnetic field. The heat flux of the FP model is reduced compared with the linear model due to the nonlocal effects of electron transport. The electron distribution function at 30 μm is shown in Fig. 3. In the low temperature region, the electron distribution function has an overfilled tail, which causes the local heat flux to be greater than that predicted by the linear model. The heat flux produces a preheating at the temperature front.

The temperature profiles at 0.05 ps for a magnetic field strength of 100 kG are shown in Fig. 2 (b). In this case, the initial Hall parameters $\omega\tau$ are 0.23 and 0.09 at high and low temperatures, respectively. The value $v\tau$, which appears in the first term of the right-hand side of Eqs. (2b) and (2c), is the mean free path of the electron with velocity v. In the magnetic field, the factor $(1 + \omega^2\tau^2)^{-1}$ appears in the right-hand side of these equations. The "effective" mean free path [1)] is represented by $l = v\tau/(1 + \omega^2\tau^2)$. The effective mean free path is the moving distance parallel to the temperature gradient within the collision time. At this magnetic field strength, the Hall parameters are sufficiently small relative to unity and Figs. 2 (a) and 2 (b) show small differences of the temperature profiles. Although the Hall parameter becomes larger than unity for high-energy electrons, the effective mean free path is still longer than the scale length of the temperature gradient. Therefore, at this magnetic field strength, the effect of the magnetic field on the nonlocal electron heat transport is small.

Figure 2 (c) shows the temperature profiles at 0.5 ps for a magnetic field strength of 1 MG. In this case, the initial values of the Hall parameters are 2.3 and 0.9 at high and low temperatures, respectively. Because the Hall parameter exceeds unity, the nonlocal electron heat transport is influenced by the magnetic fields, and the difference between the results of the FP and linear models decreases. The value $(1 + \omega^2\tau^2)^{-1}$ at high temperature is 0.16. The effective mean free path of the electron at an average temperature is six times shorter than the mean free path without the magnetic fields. Assuming that the electron mean free time depends on the third power of electron veloc-

[1)] The effective mean free path is the moving distance in the direction parallel to the temperature gradient within collision time. The mean free path l_{mfp} of the particles of the speed v and the collision frequency ν is given by $l_{\mathrm{mfp}} = v\int_0^\infty e^{-\nu t}dt = v\tau$, where $\tau = 1/\nu$. The effective mean free path l_{eff} of the electron, which changes movement direction owing to the cyclotron motion, is given by

$$l_{\mathrm{eff}} = v\int_0^\infty e^{-\nu t}\cos(\omega t)dt = \frac{v\tau}{1 + (\omega\tau)^2}.$$

Because τ is almost proportional to v^3 in the plasma, the effective mean free path of the electron with velocity higher than a certain value becomes shorter as the velocity increases.

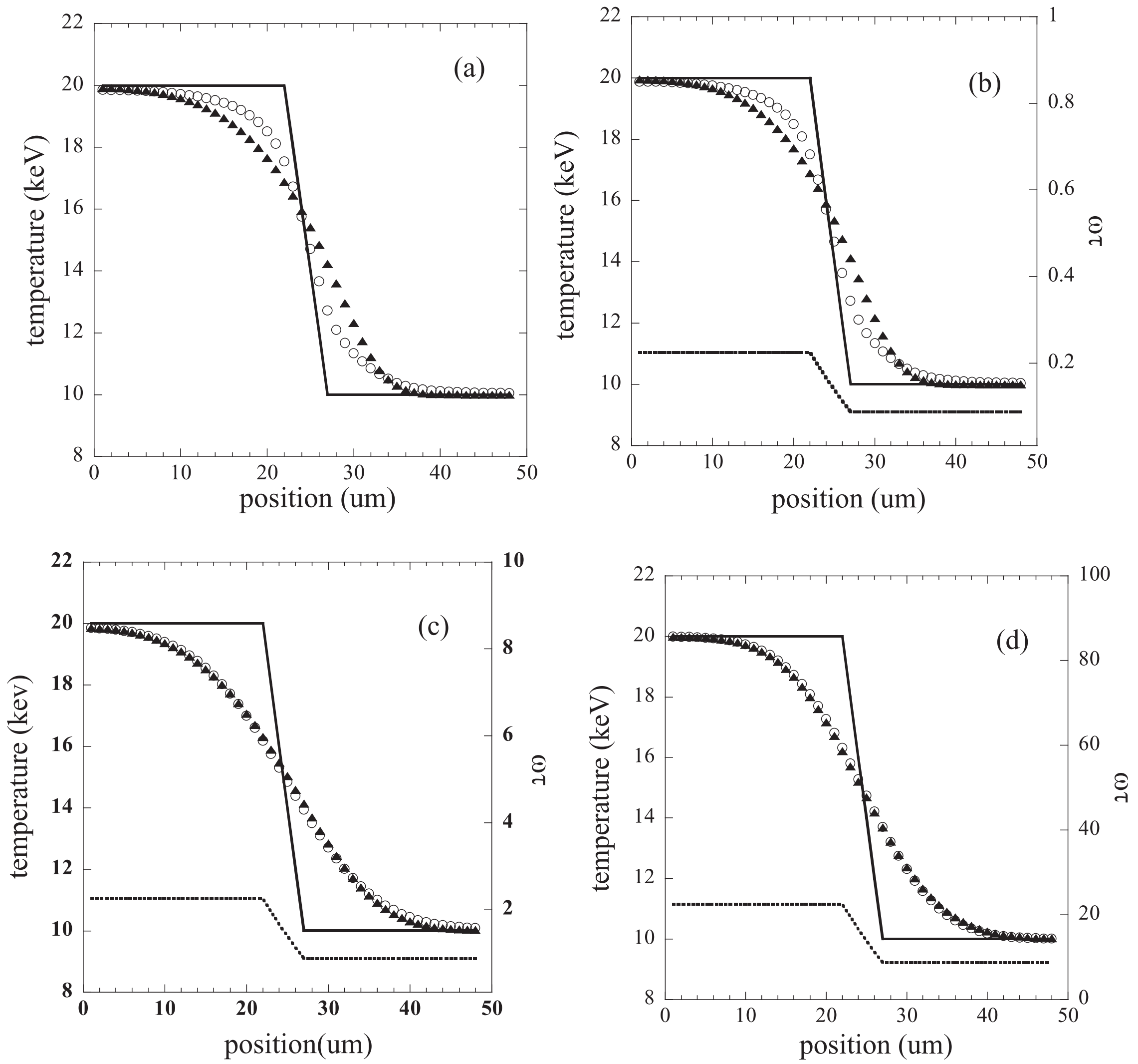

Fig. 2 The temperature profiles given by the FP and linear models at 0.05 ps for $B = 0$ G (a) and $B = 100$ kG (b), and at 0.5 ps for $B = 1$ MG (c), and 10 ps for $B = 10$ MG (d), respectively. The initial temperature profile is denoted by a solid line. The FP results are shown by circles and the linear model results are shown by filled triangles. The dotted line shows the initial $\omega\tau$ value.

ity, the effective electron mean free pass is the longest at $\omega\tau \approx \sqrt{2}$ [2)]. For high-energy electrons, the mean free time becomes longer, whereas the effective mean free path shortens depending on $v\tau/(1+\omega^2\tau^2)$, as shown in Fig. 5. At $B = 1$ MG, the maximum value of the effective mean free path is about 1 μm. The mean free path of all electrons becomes shorter than the scale length of the temperature gradient and the nonlocal effect decreases. However, for the nonlocal effect to disappear, the mean free path of all electrons must become much shorter than the scale length of the temperature gradient. Therefore, the nonlocal effects do not vanish completely, and the characteristic foot of the temperature front is observed, as shown in Fig. 2 (c).

The temperature profile for strongly magnetized plasma, where the strength of the magnetic field is 10 MG, is shown in Fig. 2 (d). The initial Hall parameters are 23 and 9 at high and low temperatures, respectively. The electron distribution functions at 30 μm are shown in Fig. 4. For strongly magnetized plasma, the temperature profile of the FP and linear models agree, and the electron distribution function becomes almost Maxwellian. At $B = 10$ MG, the maximum effective mean free path is about 0.05 μm, as shown in Fig. 5. The mean free path of all electrons becomes much shorter than the scale length of the temperature gradient; thus, a classical diffusion model can be used even for high-energy electrons.

The relation of the strength of the magnetic field and the nonlocal effect of the electron heat transport is shown in Figs. 6 (a) and 6 (b). The dependence of the limitation factor to the magnetic field strength is shown in Fig. 6 (a). The limitation factor is a coefficient by which the thermal conductivity is multiplied such that the total heat flux according to the linear model should resemble that of the FP

[2)] Assuming $\tau = \tau_0 v^3$, effective mean free path can be written as $\tau_0 v^4/(1+\omega^2\tau_0^2 v^6)$. The derivative of this value with respect to v becomes zero and the effective mean free path takes a maximum value at $\omega\tau = \sqrt{2}$.

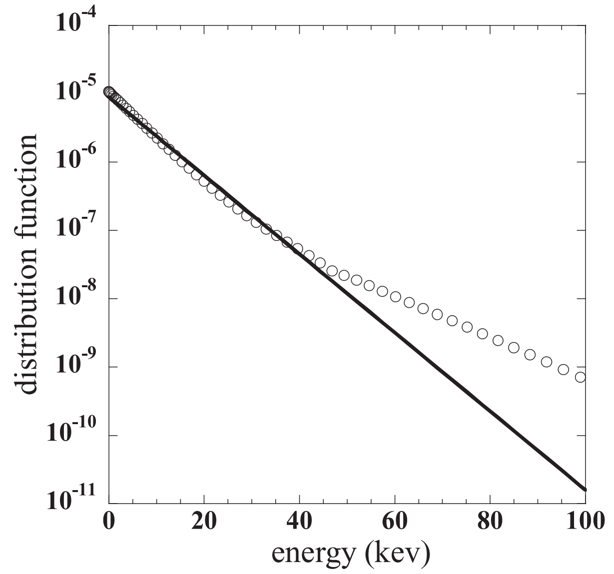

Fig. 3 Circles show the electron distribution function at 30 μm. The electron distribution function has an overfilled tail. The solid line shows the Maxwell distribution at the corresponding temperature ($T_e = \int 1/2m^2 f_0 dv^3$ in the FP model).

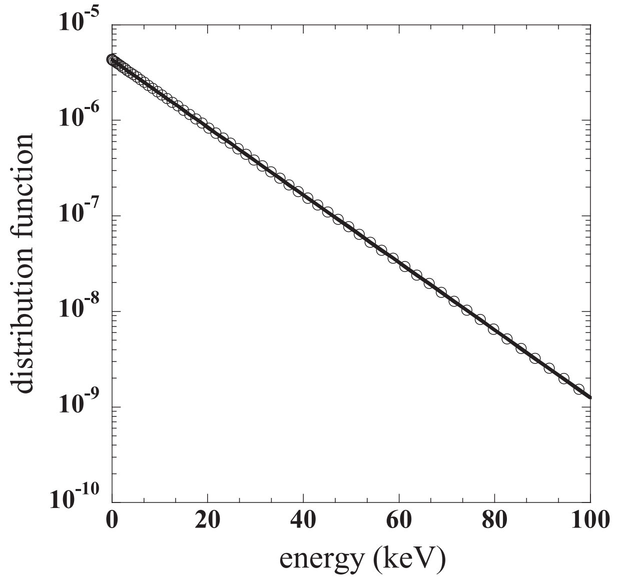

Fig. 4 The electron distribution function at 30 μm for a magnetic field strength of 10 MG. The circles denote the distribution function at 10 ps. The solid line represents the Maxwell distribution at the corresponding temperature ($T_e = \int 1/2m^2 f_0 dv^3$ in the FP model).

model at 25 μm. When $\omega\tau$ exceeds two, the amount of heat flow according to the FP model agrees with the heat flow value of the linear model. The ratio of the effective mean free path and the scale length of the temperature gradient is shown in Fig. 6 (b). The effective mean free path becomes about 1/6 of the scale length of the temperature gradient at

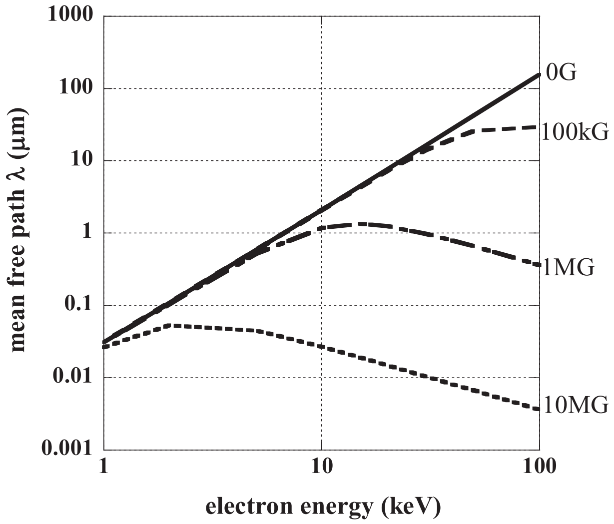

Fig. 5 Dependence of the effective electron mean free path on the magnetic field strength. The electron density is 10^{24} cm^{-3}.

1 MG, and the heat flux limitation due to the nonlocal effect disappears. It seems that the nonlocal effect disappears in the longer mean free path compared with the case without a magnetic field. The nonlocal effect in the magnetic field is decreased because the effective mean free path of high-energy electrons shortens, as shown in Fig. 5. In this case, the effective mean free path of the important heat carriers is shorter than 1 μm.

In the magnetic field, the electron mean free path does not exceed the Larmor diameter [3]. If the Larmor diameter is sufficiently shorter than the scale length of the temperature gradient, high-energy electrons tend to behave like collisional electrons. As a result, the nonlocal effect on electron transport decreases. For strongly magnetized plasma, the effective mean free paths of all electrons become shorter than the scale length of the temperature gradient, and the electron heat transport agrees well with the classical diffusion model. Moreover, the electron distribution functions agree well with the Maxwellian distribution locally. Whether a nonlocal model is required for the electron transport in magnetized plasmas is inferred by comparing the scale length of the temperature gradient and the effective mean free path, as shown in Fig. 5.

In summary, the electron heat transport in magnetized plasmas was studied using the nonlinear FP model with a magnetic field of variable strength. The dependence of the nonlocal electron heat transport on the magnetic field strength was specified. The nonlocal effect on electron transport can be estimated by comparing the effective mean free path with the scale length of the temperature gradient. Under a strong magnetic field, the electron heat transport

[3] An electron moves along with the circumference including the colliding points after collisions. Therefore, the next colliding point is on this circumference. The distance of the two colliding points is the mean free path and is shorter than the Larmor diameter.

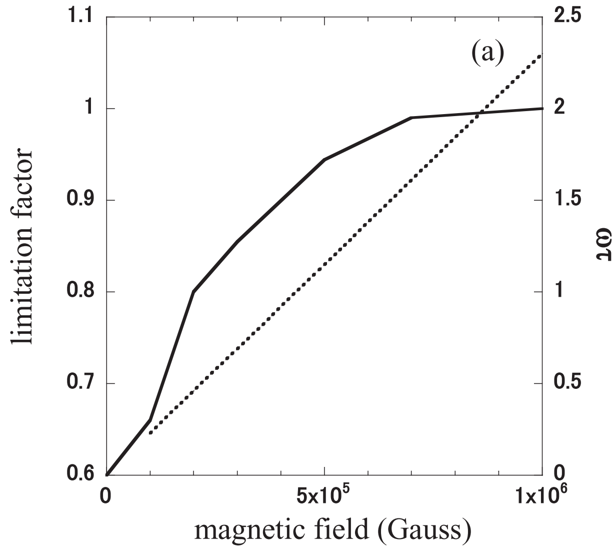

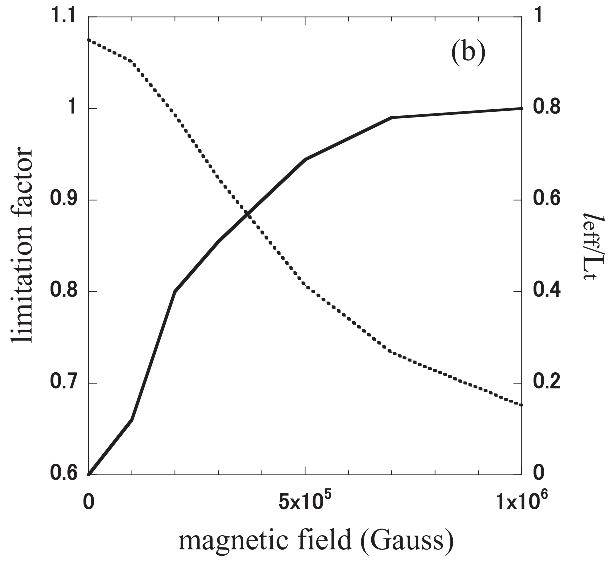

Fig. 6 Dependence of the limitation factor (solid line in Figs. 6 (a) and 6 (b)), $\omega\tau$ (dotted line in Fig. 6 (a)), and the ratio of the effective mean free path and the scale length of the temperature gradient (dotted line in Fig. 6 (b)) on the magnetic field strength.

agrees well with the results of the linear model for any energy range. In the magnetic field, the electrons move at a drift speed of the guiding center of the cyclotron motion, and the effective electron mean free path becomes shorter than the scale length of the temperature gradient in strong magnetic fields. The electron distribution functions tend to become almost Maxwellian locally under a strong magnetic field.

[1] J.A. Stamper, K. Papadopoulos, R.N. Sudan, S.O. Dean, E.A. Mclean and J.M. Dawson, Phys. Rev. Lett. **26**, 1012 (1971).
[2] T. Okada, T. Yabe and K. Niu, J. Phys. Soc. Jpn. **43**, 1042 (1977).
[3] C.E. Max, W.M. Manheimer and J.J. Thomson, Phys. Fluids **21**, 128 (1978).
[4] K. Mima, T. Tajima and J.N. Leboeuf, Phys. Rev. Lett. **41**, 1715 (1978).
[5] Y. Sakagami, H. Kawakami, S. Nagao and C. Yamanaka, Phys. Rev. Lett. **42**, 839 (1979).
[6] T. Mochizuki, T. Yabe, K. Mima, K. Yoshikawa, H. Azechi, A. Kikuchi and C. Yamanaka, Jpn. J. Appl. Phys. **19**, L645 (1980).
[7] M.G. Haines, Phys. Rev. Lett. **47**, 917 (1981).
[8] M.H. Emery, J.H. Gardner and J.P. Boris, Plasma Physics and Controlled Nuclear Fusion Research 1984, Vol.3, p.129, Nucl. Fusion Suppl. (1985).
[9] A. Nishiguchi, T. Yabe and M.G. Haines, Phys. Fluids **28**, 3683 (1985).
[10] F. Hattori, H. Takabe and K. Mima, Phys. Fluids **29**, 1719 (1986).
[11] M. Tatarakis *et al.*, Phys. Plasmas **9**, 2244 (2002).
[12] T.H. Kho and M.G. Haines, Phys. Rev. Lett. **55**, 825 (1985).
[13] J.F. Luciani, P. Mora and A. Bendib, Phys. Rev. Lett. **55**, 2421 (1985).
[14] T.H. Kho and M.G. Haines, Phys. Fluids **29**(8), 2665 (1986).
[15] A.V. Brantov, V.Yu. Bychenkov, W. Rozmus, C.E. Capjack and R. Sydora, Phys. Plasmas **10**, 4633 (2003).
[16] A.R. Bell, R.G. Evans and D.J. Nicholas, Phys. Rev. Lett. **46**, 243 (1981).
[17] J.P. Matte and J. Virmont, Phys. Rev. Lett. **49**, 1936 (1982).
[18] J.R. Albritton, Phys. Rev. Lett. **50**, 2078 (1983).
[19] R.J. Mason, Phys. Rev. Lett. **47**, 652 (1981).
[20] D.J. Bond, Phys. Lett. **A88**, 144 (1982).
[21] A.B. Langdon, Proc. 1981 Centre European de Calcul Atomique et Moleculaire Workshop on The Flux-Limiter and Heat Flux Instabilities in Laser-Fusion Plasmas (Universite Paris Sud, France, 1981) p.69.
[22] S.I. Braginskii, *Reviews of Plasma Physics* **1** (Consultants Bureau, New York, 1965).